RSC Advances

ROYAL SOCIETY OF CHEMISTRY

www.rsc.org/advances

Synthesisand electrochemical performance of Ni and F doped $LiMn_2O_4$ cathode materials

QingingWang,[a]XiushengZhang,[a]*YunlongXu,*[a] Dong Liu,[b]HuiDong,[a]Yang Zhang [a]

Abstract

The series of Ni and F ion doped $LiMn_2O_4$ composite cathode materials are synthesized via a sol-gel method with citric acid as the chelating agent.Themorphology and structure of $LiNi_xMn_{2-x}O_{4-y}F_y$were characterized byXRD,SEM,EDSand the electrochemical performance were tested and characterized by CV andEIS.The results showed that Ni and F ions were uniformly dispersed in lattice without changing the structure andmorphology of $LiMn_2O_4$.$LiNi_{0.03}Mn_{1.97}O_{3.95}F_{0.05}$ exhibitsan excellent electrochemical performanceamong all the samples, and delivers initial discharge capacity of 120.3mAhg^{-1}at 1 C and with the retention of 94.5% (25°C) and 80.4% (55°C) after 100th cycle respectively.The results demonstrated that the dual-doping of Ni and F ion in lithium manganate can prevent the manganate from dissolving in the electrolyte and enhanced the cycling performance at elevated temperature,exhibiting excellent performance at different discharge rates.

Introduction

With the depletion of traditional fossil fuels such as coal and oil and deteriorating

environment, the exploration and utilization of new energy type such as lithium-ion battery are receiving more and more attention.[1-4]Under the intensive study worldwide,the cathode is generally regarded as the capacity-determiningcomponent of a LIB. Ideally, the cathode should deliver highspecific capacity, high operating voltage, low cost, superior safetyand long cycle life within a wide working temperature range inorder to meet the requirements for applications.[5, 6]Among numerous cathodematerials being studied, spinel $LiMn_2O_4$ is one of the most promising candidates to meet the above requirements.[7, 8]

However, spinel$LiMn_2O_4$suffers from severe capacity decay after long-term cycling and deprived rate capability under high rates, particularly at elevated temperatures.[9, 10]Researchers discovered a series of causes contributing to the capacity fading: (i) Gradualmanganate deficiency because of the dissolution of Mn^{3+} to the active electrolyte via disproportionation reaction.[11, 12] (ii) The degradation of the electrolyte $LiPF_6$, whose decomposition leads to accelerated dissolution of Mn^{3+} and electrode active material.[13, 14] (iii) Jahn-Teller distortion of the cubic spinel structure of $LiMn_2O_4$ during the battery charge/discharge.[15]

In order to mitigate these problems, various approaches such as doping and electrode surface coating,[16]have been proposed and employed and remarkable results were achieved by doping different elements in the material.[17, 18]Because Mn^{3+} is known to be responsible for manganese dissolution and Jahn-Teller distortion, many attempts have been made to substitute small amounts of Mn^{3+} with other metal cations.

Manyresearchgroupshave investigated the properties ofmanganese-substituted spinels $LiM_xMn_{2-x}O_4$ (M = Al, Cr,Ti, Fe, Co, Zn, Mg) and it shows that doping can efficiently improve the cathode materials electrochemical properties.[19-23] Chen announced that $La^{2+}$and F^-could replace the $Mn^{3+}$and O^{2-}in $LiMn_2O_4$ structure and strengthen the structural stability of spinel.[24] Ben-Lin reported that substitution of manganese by aluminum decreases the unit cell volume and the decrease of Mn^{3+} concentration reduces the Jahn–Teller distortion and also stabilizes the structure integrity of the active, improved electrochemical stability.[25, 26] Although there are plenty of doping modification methods in references aimed to improve the electrochemical property of $LiMn_2O_4$ materials, most of them were simplex cation or anion doping and the doping of Ni and F still remain in skimp and worth study. We considered if the Ni and F dual-doping can further enhance the electrochemicalperformance and in this study, Ni and F ions were adopted as the doping elements in $LiMn_2O_4$ and obtained a preferable modification result.

In this study, we conducted the recombine doping of Ni and F to $LiMn_2O_4$ materials modification research and synthesized several of dual-doped $LiNi_xMn_{2-x}O_{4-y}F_y$ via a sol-gel method. We studied the effect of F Ni ions dual-doping to the $LiMn_2O_4$ materials on its structure and electrochemical properties systematically and obtained the best doping ratio of F Ni ions. It turned out that F and Ni ions dual-doping can improve the cycling stability and discharge performance under the high-rate of $LiMn_2O_4$.

Experimental section

Sample preparation

The stoichiometric amount of $Li(OH)\cdot H_2O$ (Sinopharm Chemical Reagent Co.Ltd, Shanghai) and LiF (Aladdin Industrial Inc., Shanghai) were firstly dissolved in deionized water at 50°C and then $C_6H_8O_7\cdot H_2O$ (Shanghai China Lithium Industrial Co. Ltd, Shanghai) was added into such solution as the chelation agent. $C_4H_6NiO_4\cdot 4H_2O$ (Chemical Reagent Co. Ltd, Shanghai) and $C_4H_6MnO_4\cdot 4H_2O$ (Sinopharm Chemical Reagent Co. Ltd, Shanghai) were slowly added into the solution and heated to 80°C under vigorous stirring. During the stirring, $NH_3\cdot H_2O$ (Chemical Reagent Co. Ltd, Shanghai) was used to adjust the pH value of the above solution. After the pH reaches to 8, the mixture appeared as a red brown sol.Then the sol was dried in a microwave oven (2.5 GHz, 500 W) until a transparent gel was obtained. After fully grinding, thegel wastransferred to a tube furnace and pre-heated at 400 °C for 3h,followed by the calcination at 800°C for 10 h in ambient atmosphere.The heating rate and cooling rate used in the heat treatment were both 2 °C/min. After the calcination, the black dual-doped spinel $LiNi_xMn_{2-x}O_{4-y}F_y$ (x=0, 0.01, 0.03 and y=0, 0.03, 0.05) powder was achieved. In order to study the effect of doping, various samples $LiMn_2O_4$, $LiMn_2O_{3.95}F_{0.05}$, $LiNi_{0.03}Mn_{1.97}O_4$, $LiNi_{0.01}Mn_{1.99}O_{3.97}F_{0.03}$, $LiNi_{0.01}Mn_{1.99}O_{3.95}F_{0.05}$, $LiNi_{0.03}Mn_{1.97}O_{3.97}F_{0.03}$ and $LiNi_{0.03}Mn_{1.97}O_{3.95}F_{0.05}$ were synthesized and they are denoted as 0N-0F, 0N-5F, 3N-0F, 1N-3F, 1N-5F, 3N-3F and 3N-5F for the sake of discussion. The pure

$LiMn_2O_4$ was also synthesized under the same condition for the control experiment.

Sample characterization

Powder X-ray diffraction (XRD, D/MAX, 2550V, Japan) using Cu K_α radiation (λ= 1.54056Å) was used to identify the phase composition of synthesized materials and MDI Jade software was used to calculate the lattice parameters. The field emission scanning electron microscopy (FE-SEM, Hitachi S-4800, Japan) was used to evaluated the morphology and the distribution while species of the elements were analyzed by energy dispersive spectrometer (EDS).The electrochemical performance of the synthesized material wasevaluated by assembling CR2032 coin cells. The cathode slurrywas firstly prepared by dispersing 80 wt. % active material, 10 wt. % acetylene black (Shanghai Haohua Chemical Co. Ltd, Shanghai) and 10 wt. %polyvinylidene fluoride (PVDF, Shanghai Ofluorine Chemical Technology Co. Ltd, Shanghai) in N-methyl-2-pyrrolidone (NMP, Sinopharm Chemical Reagent Co. Ltd, Shanghai) solvent and coated onto Al foil, then dried in a vacuum oven at 120℃ for overnight. Lithium foil was used as the counter electrode and Celgard 2400 microporous polyethylene membrane as the separator.1 M $LiPF_6$ in ethylene carbonate (EC) and diethyl carbonate (DEC) (1:1, V/V) (Guangzhou TinciMaterialt Technology Co. Ltd, Guangzhou) was used as the electrolyte. The cells were assembled in an argon-filled glove box and left to age for 12 h before the charge/discharge test performed on a battery test instrument(CT2001A, LAND Battery Program-control Test System, China) over the voltage range of 3.0-4.4V(vs Li/Li^+) at both room

temperature(25°C) and elevated temperature (55°C). Cyclic voltammetry (CV) was performed between 3.0-4.4 V on an electrochemical workstation (CHI660D, Shanghai Chenhua Co. Ltd., China) at the scan rate of 0.1mV/s. Electrochemical impedance spectroscopy (EIS) of the cells was also potentiostatically conducted on anelectrochemical workstation (CHI, 660B, CHENHUA, China) between 10^{-2} and 10^{5} Hz with an AC oscillation amplitude of 5 mV to investigate the charge transfer of synthesized materials. The collected EIS spectra were fitted using ZSimpWin software.

Results and discussion

Structure and morphology

The X-ray diffraction patterns of various synthesized dual-doped $LiNi_xMn_{2-x}O_{4-y}F_y$(x=0, 0.01, 0.03y=0, 0.03, 0.05) are shown in Fig. 1. The diffraction peaks of all samples are in accordance with the diffraction pattern of the cubic spinel structure $LiMn_2O_4$ (JCPDScard No. 35-782) with the Fd-3m space group. All samples show the same diffraction patterns and the doping of Ni and F ions do not appear to affect the crystal structure of the samples.[27] No impurity peaks were detected as well. This indicates that the $Ni^{2+}$and F^{-}substitutinghave seated at $Mn^{3+}$and O^{2-}site in $LiMn_2O_4$ and thus no other phaseis formed.

Rietveld refinement of the XRD data of the samples is carried out and the result is shown in Fig. 2. Table1 shows the crystal parameters of various synthesized samples calculated from the XRD patterns. The structuralinformation can be found in

Tables 1. According tothe Fig. 2, as well as the R factors in Table 1, the calculated curve (black) matches well with the experimental data(red) which confirmed that the samples are coincident with thediffraction pattern of$LiMn_2O_4$.

As can be seen from Table1, that the doping of Ni^{2+} leads to the shrinkage of lattice parameter and the doping of F^- goes to the opposite result. It was mainly attributed to the increase of average valence of manganese due to the Ni^{2+} doping while the radius of Mn^{4+} (0.067nm) is smaller than the radius of Mn^{3+} (0.072nm) meanwhile the energy of Ni^{2+} site preference is higher, thus forming the stronger bond of Ni-O after doping which leads to the shrinkage of cell volume and the decreasing of lattice parameters.[28]The radius of F^- is smaller than the O^{2-} which indicates that the lattice parameters should be decreased with the amount of F^- doping according to the Vegard rules, but the average valence would be decreased due to the doping of F^- which increase the content of Mn^{3+} causing the augment of lattice parameters.[18] The lattice parameters were joint influenced by the Ni^{2+} and F^- doping for the dual-doping samples and the lattice parameters of different doping ratio demonstrated that the Ni^{2+} and F^- ions were doped into the structure cell of $LiMn_2O_4$ further.

Fig. 3 shows the FE-SEM images of the pristine $LiMn_2O_4$sample and doped $LiNi_xMn_{2-x}O_{4-y}F_y$ (x=0.03, y=0.05) sample.Both samples have uniform and nearly polyhedral structure morphology and all particles show a quite uniform distribution with the size ranging from 100 to 500 nm. The elemental mapping of the $LiNi_xMn_{2-x}O_{4-y}F_y$ sample by EDS was given in Figure4 where 4a shows the integral

distribution of the observed element O, Mn, Ni and F and 4b and 4c represent the SEM image of selected test area and the mapping result of individual elements respectively. As shown in Figure4b, all observed elements have homogeneous distributions, which suggests that Ni^{2+} and F^- ions were doped into $LiMn_2O_4$ crystal structure uniformly via the sol-gel route.

Electrochemical measurements

In order to investigate the impact of dual-doped of Ni^{2+} and F^- ions on the electrochemical performance of $LiMn_2O_4$ cathode material, the constant charge-discharge test was carried out on the synthesized samples. Figure 5 shows the initial charge/discharge profile of pristine and doping $LiMn_2O_4$ samples at 1 C between the potential range 3.0-4.3 V (vs Li/Li^+) at room temperature. There are two voltage platformsonboth charge and discharge curves of all samples,representing the typical electrochemical performance of single-phased spinel $LiMn_2O_4$structure. It shows thatthe doping of Ni^{2+} and F^- ions have no impact on the charge/discharge profile of the doped $LiMn_2O_4$ material. As seen from Figure5, the doping of Ni^{2+}intends to lower the discharge capacity. This is because of the Ni^{2+}ion insertion to the 16d site of $LiMn_2O_4$ unit cell, causing the increase of manganese average valence and the decrease of Mn^{3+}ions electrochemical activity. However, the F^- ions dopingmainly appears toincrease the discharge capacity due to the insertion of the F^- ions into the 32e sites partially replacing the O^{2-}, leading to the decrease of manganese average valence andthe increaseof Mn^{3+} ions electrochemical activity.Meanwhile, the

radius of F^-ion is smaller than O^{2-} ion, which enables easier replacement ofoxygen atom by F^- ions.This in turn, will broaden insertion/extraction channels of Li^+ions and enhance its migration rate and thus increase the discharge capacity of $LiMn_2O_4$cathode material. The charge-discharge capacity were influenced by the doping of $Ni^{2+}$and F^- together and range from sample (0N-5F) to sample (3N-0F).In conclusion, the doping of Ni^{2+} leads to the reduction of capacity to a certain degree while doping the F^- would promote the capacity and the dual-doping of $Ni^{2+}$and F^- can remedy the capacity loss of the single doping of Ni^{2+}.The results show that the (3N-5F) was the optimumratio for its electrochemical performance.

The long-term cyclic performance of all synthesized $LiMn_2O_4$samples was firstly evaluated at room temperature (25°C) under 1 C charge/discharge rate and the results are exhibited in Fig. 6. Clearly, the improvement on the battery cyclic performance was achieved onall doped samples and the dual-doped samples even show more superior capability than un-ion doped samples. Especially, the 3N-5F sample delivers the highest capacity retention ratio (94.5%) while the pristine $LiMn_2O_4$, 0N-5F and 3N-0F samples preserveonly 77.8%, 86.7% and 88.3% capacity retention ratio respectively. It is expected that the dual-doped sample might possess better crystal structure stability to realize higher electrochemical performance.[29]Such structure stablization of $LiMn_2O_4$ stems from two contributions: (i) stronger bond strength ofthe Ni-O(1029kJ/mol) than it of the Mn-O bond (946kJ/mol), which is expected to mitigate Jahn-Teller structure distortion effect, (ii) larger electronegativity thus greater

attraction force, of F^- ions than O^{2-} ionsto thecations.Note that slightly higher capacity retention achieved on single Ni doped sample (3N-0F) than single F doped sample (0N-5F)is likely due to increased Mn^{3+}amount which results in aggravated Jahn-Teller effect regardless of the enhanced structure stability by F doping.[30]However, the dual-doped sample (3N-5F) manifests a synergistic effect to improve the electrochemical performance of $LiMn_2O_4$ compared to either undoped sample or single ion doped sample. .

We also studied cyclic performance of doped samples at elevated temperature (55 °C) under 1C discharge rate and the results are revealed in Fig.7. As expected, all samples tested, especially undoped $LiMn_2O_4$, show inferior long-term cyclic performance at elevated temperature than when they were tested at room temperature.This is mainly because of aggravated Jahn-Teller effect caused by the high temperature along with the dissolution of Mn^{3+}.[7] Compared to undoped sample however, all doped sample show great improvement in terms of the capacity retention. To further elaborate, the first and 100^{th} cycle discharge capacitytogether with the capacity retention ratio of all tested samplesat both room and elevated temperatures are summarized in Table 2. Similar as its remarkable long-term cyclic performance at room temperature, the Ni and F dual-doped sample (3N-5F) exhibits the highest capacity retention rate (80.4%) even at elevated temperature. It is suspected that the synergistic effect of dual-doping, which suppresses the Jahn-Teller effect and the dissolution of Mn^{3+}, leads to more stable crystal structure of $LiMn_2O_4$ and therefore

enhanced long-term cyclic performance at both room and elevated temperatures.[29, 31-33]This further proves that dual element doping may be rendered as an effective approach to elongate the long-term cyclic performance of $LiMn_2O_4$ material.

Whether the battery material maintains significant capacity under high discharge rate is another criteria to rationalize doped $LiMn_2O_4$ samples with high electrochemical performance. To this end, the high rates (1C, 2C, 5C, 10C, 20C) cyclic performances of various doped samples were carried out and the results are as shown in Fig. 8. All samples displaydeteriorated capacity as the discharge current increases. This is well-known due to delayed/unaccommodated migration rate of Li ion as a result of abrupt extraction force subject to high discharge rate, i.e., high electrode polarization.[33] When comparing the discharge capacity of all samples at high rates, the dual-doped sample (3N-5F) exhibits the best rate capability, delivering 118.4 $mAhg^{-1}$, 115.3 $mAhg^{-1}$, 110.5 $mAhg^{-1}$, 102 $mAhg^{-1}$ and 90.5 $mAhg^{-1}$ at 1C, 2C, 5C, 10C and 20C respectively of the constant discharge capacity and it was 90.5$mAhg^{-1}$ even at 20C while the pristine $LiMn_2O_4$ declined to 75.8$mAhg^{-1}$.It can be seen that the capacity of the dual-doped sample (3N-5F) can recover to the initial value as long as the current density reverses back to a low rate. As the high discharge rate also causes electrode resistance ohmicpolarization that reduces the electronic conductivity of the active material,it is believed that the synergistic effect of Niand F dual-doping not only increases the migrationrate of Li ion inside the active materials, but also gives rise to enhanced electronic conductivity, thus superior high rate

electrochemical performance.

The high rates (1C, 2C, 5C, 10C, 20C) cyclic performances of various doped samples at elevated temperature (55 °C) were carried out and the results are as shown as Fig. 9. All samples showeddeteriorated capacity as the discharge current increases at elevated temperature. It can be seen that the dual-doped sample (3N-5F)exhibits the best rate capability among the samples and it was 78.9mAhg^{-1} even at 20Cwith abit ofcapacity fading when it returned to 1C. Note thatthe capacitiesfading on all samples under high dischargerate and temperature are due totheaggravated Jahn-Teller effect and the Niand F dual-doping can suppresses the Jahn-Teller effect and the dissolution of Mn^{3+} leading to the preferable electrochemical property.

Electrochemical impedance spectroscopy (EIS) was further performed on various samples at certain periods of time (the 1st, 25th, 50th, 75th and the 100th cycles) during long-term cycle to probe the charge transfer kinetics within the battery material. The Nyquist plots along with the fitted equivalent circuit of the samples were shown in Fig. 10 and Table 3. In Fig.10a, a high-frequency semi-circle and a low-frequency slope are seen as the typical spectrum of $LiMn_2O_4$ material.The semicircle in the high frequency region isattributed to dual-effect of the interface impedance that Li ions migration through the SEI film (R_f) along with the charge transfer resistance (R_{ct}) while the inclined line in the low frequency region represents the Warburg impedance (W),[31] which is associated with the diffusion of Li ion in electrode. It can be seen from Table 3 that the values of R_{ct} for the doped samples are much lower than the

undoped sample in despite of slight change of film resistance R_f. This is especially true for the dual-doped sample (3N-5F). On the other hand, the great reduction of Warburg impedance on doped samples over undoped one is an indicative of easier Li ion diffusion in bulk electrode materials.[34] The above analysis is especially true for Ni and F dual-doped sample as it is capable of dwindling the charge transfer resistance and Warburg impedance by 62% and 53% respectively compared to pristine $LiMn_2O_4$ sample. This is believed due to increased migration rate and expanded diffusion channels for Li ions through Ni and F dual-doping and thus better electrochemical performance. Such finding is corroborated with Fig. 10b that shows the impedance growth rate of pristine $LiMn_2O_4$ isconsiderably higher than the doped samples, indicating that the doping would strengthen the structure stability of $LiMn_2O_4$ material and lead to more admirable electrochemical performance.[24] Note that the EIS results are in good agreement with previous charge/discharge characteristic results of all samples.

In order to explore the effect of dual-doping of Ni^{2+} and F^- on spinel $LiMn_2O_4$, the typical cyclic voltammograms of the samples were performed using lithium as a counter and reference electrode in the voltage range of 3.0-4.4 V at a scan rate of $0.1mVs^{-1}$ as shown in Fig. 11. The two obvious redox peaks were observed in all the samples stating that the insert-extract reaction of Li ion ended in two parts which conformed to the distinct characteristics of spinel $LiMn_2O_4$ and attested that the doping would not change its structure and reaction characteristics.[6, 18] It was observed

that the potential difference between reduction and oxidation peak decreased of the doping samples and the potential difference represents the degree of reversibility of the insert-extract reaction which indicated that the degree of reversibility of the reaction was increased.[15, 35] The results implying that the dual-doping of Ni^{2+} and F^- accelerated the diffusion velocity, enhanced the stability of $LiMn_2O_4$ crystal structure and the redox peak of the sample (3N-5F) was the sharpest demonstrating the fastest reaction velocity and the best electrochemical property which is in theaccordance with the charge-discharge performance test results. These results indicate that the dual-doping samples enhanced the electrochemical property of $LiMn_2O_4$ materials.

Conclusions

In summary, the spinel $LiMn_2O_4$ with various amounts of Ni^{2+} and F^- doping compound was successfully synthesized via a sol-gel route. The doping would not change the crystal structure and morphology, the doping ions distribution uniformly as well. The dual-doping of Ni^{2+} and F^- enhanced the electrochemical property more than the single Ni^{2+} or F^- doped samples. Compared with the other samples, the sample (3N-5F) exhibits much better cycle performance at room and elevated temperature. The capacity retention ratio were 94.5% (25°C) and 80.4% (55°C) after 100 cycles and it delivered 90.5 $mAhg^{-1}$ of the discharge capacity even at 20C rate. The dual-doping of Ni^{2+} and F^- could enhance the Li ion migration rate and structure stability ascribe to the synergistic effect of dual-doping leading to better electrochemical performance. The as-obtained results indicate the Ni^{2+} and F^-

dual-doping receive an attractive application for practical high-power Li-ion battery.

Acknowledgements

This work is supported by Shanghai Leading Academic Discipline Project (B502) and Shanghai Key Laboratory Project (08DZ2230500).

Notes and references

[a]*Key Laboratory for Ultrafine Materials of Ministry of Education, Shanghai Key Laboratory of Advanced Polymeric Materials, School of Materials Science andEngineering,East China University of Science and Technology, Shanghai 200237, P.R. China.*

[b]*Department of Materials Science and Engineering, University of Texas at Arlington, Arlington, TX 76019, USA.*

1. M. Armand and J. M. Tarascon, Nature, 2008, 451, 652-657.

2. M. S. Whittingham, Cheminform, 2004, 35, págs. 4271-4301.

3. K. Amine, J. Liu, S. Kang, I. Belharouak, Y. Hyung, D. Vissers and G. Henriksen, Journal of Power Sources, 2004, 129, 14–19.

4. E. Hosono, T. Kudo, I. Honma, H. Matsuda and H. Zhou, Nano Letters, 2009, 9, 1045-1051.

5. H. W. Chan, J. G. Duh, S. R. Sheen, S. Y. Tsai and C. R. Lee, Thin Solid Films, 2005, 200, 1330–1334.

6. D. W. Shin, J.-W. Choi, Y. S. Cho and S.-J. Yoon, Journal of Electroceramics, 2009, 23, 200-205.

7. Iguchi, Tokuda, Nakatsugawa and Munakata, Journal of Applied Physics, 2002, 2149-2154.

8. J. Wang, W. Lin, B. Wu and J. Zhao, ElectrochimicaActa, 2014, 245–253.

9. L. Xiong, Y. Xu, C. Zhang, Z. Zhang and J. Li, Journal of Solid State Electrochemistry, 2011, 15, 1263-1269.

10. W. Zhu, D. Liu, J. Trottier, C. Gagnon, A. Guerfi, C. M. Julien, A. Mauger and K. Zaghib, Journal of Power Sources, 2014, 264, 290–298.

11. R. Jiang, C. Cui and H. Ma, Physical Chemistry Chemical Physics, 2013, 15, 6406-6415.

12. J. P. Tu, H. M. Wu, Y. Z. Yang and W. K. Zhang, Materials Letters, 2007, 61, 864–867.

13. A. Yamada, Journal of Solid State Chemistry, 1996, 122, 160–165.
14. G.-M. Song, W.-J. Li and Y. Zhou, Materials Chemistry and Physics, 2004, 87, 162–167.
15. L. HW, M. P, R. R, M. CM, C. Y and K. d. K., Nano Lett., 2010, 10, 3852-3856.
16. G. D, J. JA and W. Y., Nanoscale, 2011, 3, 1465-1469.
17. L. Xiao, Y. Zhao, Y. Yang, Y. Cao, X. Ai and H. Yang, Electrochimica Acta, 2008, 54, 545–550.
18. R. Thirunakaran, R. Ravikumar, S. Gopukumar and A. Sivashanmugam, Journal of Alloys and Compounds, 2013, 556, 266–273.
19. Y.-S. Lee, N. Kumada and M. Yoshio, Journal of Power Sources, 2001, 96, 376–384.
20. D. Qian, Y. S. Meng, B. Xu and Z. Wang, Materials Science and Engineering: R: Reports, 2012, 73, 51–65.
21. T.-F. Yi, C.-Y. Li, Y.-R. Zhu, R.-S. Zhu and J. Shu, Russian Journal of Electrochemistry, 2010, 46, 227-232.
22. T. Dumont, T. Lippert, M. Döbeli, H. Grimmer, J. Ufheil, P. Novák, A. Würsig, U. Vogt and A. Wokaun, Applied Surface Science, 2006, 252, 4902–4906.
23. B. Xu, D. Qian, Z. Wang and Y. S. Meng, ChemInform, 2013, 44, 51–65.
24. M. Chen, S. Li and C. Yang, Journal of University of Science & Technology Beijing Mineral Metallurgy Material, 2008, 15, 468–473.

25. B.-L. He, S.-J. Bao, Y.-Y. Liang, W.-J. Zhou, H. Li and H.-L. Li, Journal of Solid State Chemistry, 2005, 178, 897–901.

26. M. Prabu, M. V. Reddy, S. Selvasekarapandian, G. V. S. Rao and B. V. R. Chowdari, Electrochimica Acta, 2013, 88, 745–755.

27. T. Yang, K. Sun, Z. Lei, N. Zhang and Y. Lang, Journal of Solid State Electrochemistry, 2011, 15, 391-397.

28. Q. Wei, X. Wang, X. Yang, B. Ju, B. Hu, H. Shu, W. Wen, M. Zhou, Y. Song and H. Wu, J.mater.chem.a, 2013, 1, 4010-4016.

29. J. Liu and A. Manthiram, J. Phys. Chem. C, 2009, 113, 15073-15079.

30. H. R. Lee, B. Lee, K. Y. Chung, B. W. Cho, K. Y. Lee and H. O. Si, Electrochimica Acta, 2014, 136, 396–403.

31. D. Arumugam and G. P. Kalaignan, Thin Solid Films, 2011, 520, 338–343.

32. Z. Zheng, Z. Tang, Z. Zhang, W. Shen and Y. Lin, Solid State Ionics, 2002, 148, 317–321.

33. T. F. Yi, X. G. Hu and K. Gao, Journal of Power Sources, 2006, 162, 636-643.

34. W. Wen, B. Ju, X. Wang, C. Wu, H. Shu and X. Yang, Electrochimica Acta, 2014, 147.

35. S. Zhao, Y. Bai, Q. Chang, Y. Yang and W. Zhang, Electrochimica Acta, 2013, 727–735.

Table 1 Crystal parameters of various synthesized samples

Sample	a(Å)	Space	Rwp (%)	Rp (%)
0N-0F	8.2465(2)	Fd3 m	7.48	5.14
0N-5F	8.2493(4)	Fd3 m	8.05	5.86
3N-0F	8.2386(2)	Fd3 m	6.47	4.01
1N-3F	8.2452(3)	Fd3 m	6.39	3.97
1N-5F	8.2473(5)	Fd3 m	7.16	4.86
3N-3F	8.2412(3)	Fd3 m	7.22	4.93
3N-5F	8.2435(2)	Fd3 m	8.41	6.11

Table 2 (a)The specific capacity and retention rates of various Ni^{2+} and F^-dual-doped $LiMn_2O_4$ samples at 25□.

Sample	Initial discharge capacity/$mAhg^{-1}$	100th discharge capacity/$mAhg^{-1}$	Retention rate/%
0N-0F	116.3	90.4	77.8%
0N-5F	122.5	106.2	86.7%
3N-0F	114.6	101.2	88.3%
3N-5F	120.3	113.7	94.5%

(b) The specific capacity and retention rates of various Ni^{2+} and F^-dual-doped $LiMn_2O_4$ samples at 55□.

Sample	Initial discharge capacity/$mAhg^{-1}$	100th discharge capacity/$mAhg^{-1}$	Retention rate/%
0N-0F	117.2	74.9	63.9%
0N-5F	121.1	90.6	74.8%
3N-0F	120.6	92.3	76.5%
3N-5F	127.1	102.2	80.4%

Table 3 The AC impedance analysis of various Ni^{2+} and F^-dual-doped $LiMn_2O_4$ samplesduring the first discharge.

Sample	R_f/Ω	R_{ct}/Ω	$W/\Omega cm^2 s^{-1}$
0N-0F	10.9	107.5	78.9
0N-5F	9.2	52.3	45.6
3N-0F	9.5	55.8	51.7
3N-5F	8.9	41.2	37.8

Figure Captions

Fig.1 XRD patterns of various Ni^{2+} and F^- dual-doped $LiMn_2O_4$ samples.

Fig. 2 Observed (red) and calculated (black)XRD patterns for the (3N-5F) sample. The tick marks represent the position of all possible Bragg reflections of $LiMn_2O_4$.

Fig. 3 SEM images of(a) pristine $LiMn_2O_4$ sample and (b) (3N-5F) sample.

Fig.4EDS mapping result of the $LiNi_{0.03}Mn_{1.97}O_{3.95}F_{0.05}$ sample.

Fig.5 Initial charge-discharge curves of various Ni^{2+} and F^- dual-doped $LiMn_2O_4$ samples.

Fig. 6 Cyclic performances of Ni^{2+} and F^-dual-doped $LiMn_2O_4$ samples at rate of 1C at room temperature (25 °C).

Fig. 7 Cyclic performances of Ni^{2+} and F^- dual-doped $LiMn_2O_4$ samples at rate of 1C at elevated temperature (55 °C).

Fig.8 Rate performance of various Ni^{2+} and F^-dual-doped $LiMn_2O_4$ samples at room temperature (25 °C).

Fig. 9 Rate performance of various Ni^{2+} and F^-dual-doped $LiMn_2O_4$ samples at

elevated temperature (55 °C).

Fig. 10 (a) The Nyquist plots of various Ni^{2+} and F^- dual-doped $LiMn_2O_4$ samples during the first discharge (b) impedance changes with cycle.

Fig.11 CV curves of various Ni^{2+} and F^- dual-doped $LiMn_2O_4$ samplesduring the first discharge.

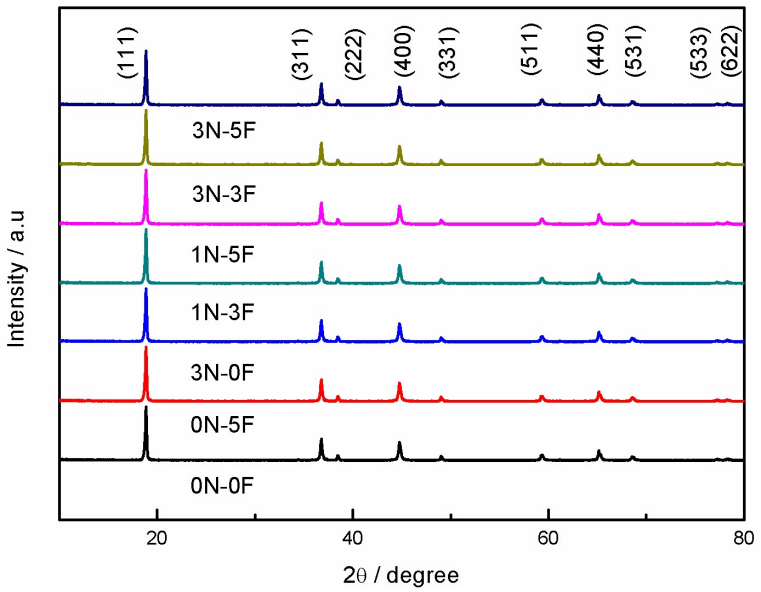

Fig. 1 XRD patterns of various Ni^{2+} and F^- dual-doped $LiMn_2O_4$ samples.

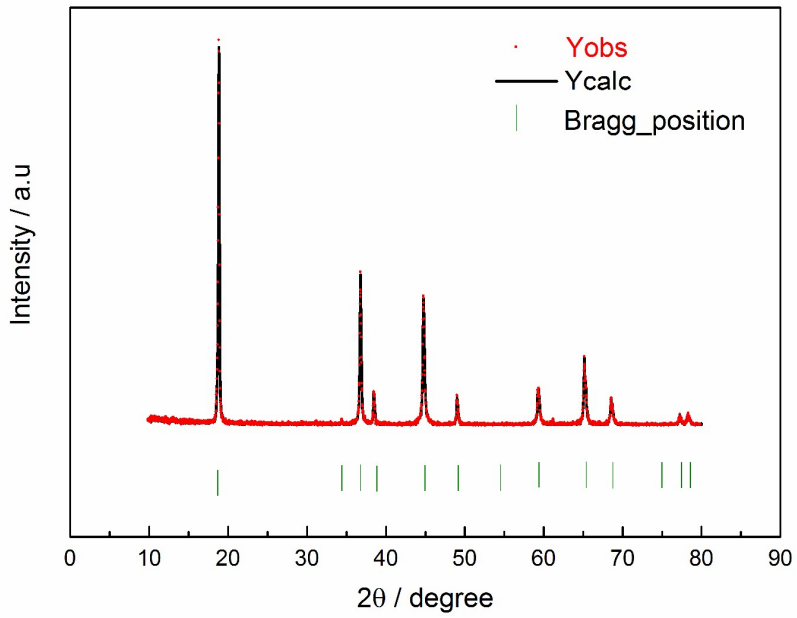

Fig. 2 Observed (red) and calculated (black)XRD patterns for the (3N-5F) sample. The tick marks represent the position of all possible Bragg reflections of $LiMn_2O_4$.

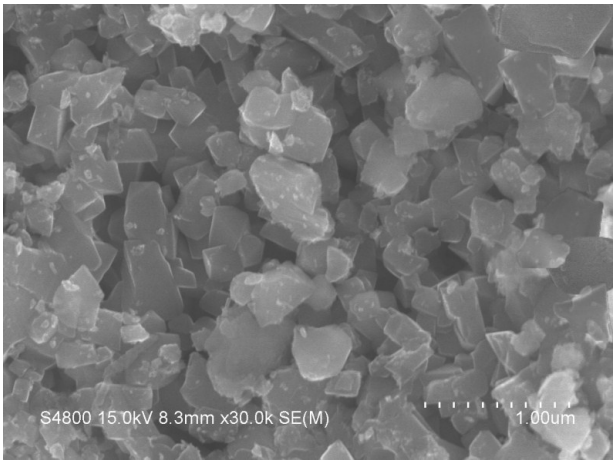

(a)

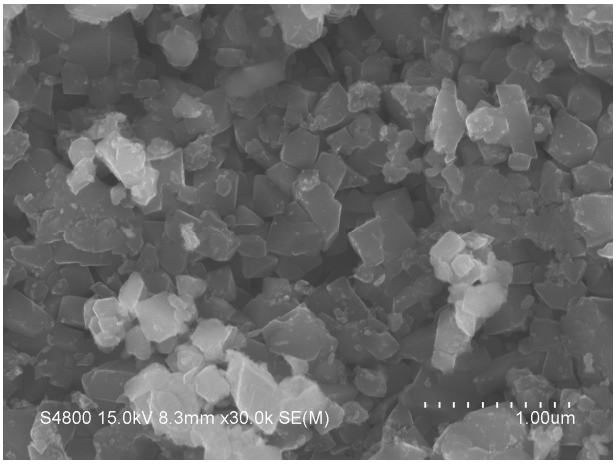

(b)

Fig. 3 SEM images of (a) pristine $LiMn_2O_4$ sample and (b) (3N-5F) sample.

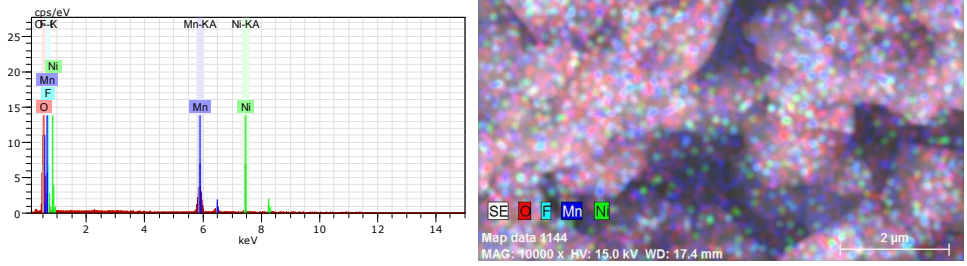

(a) (b)

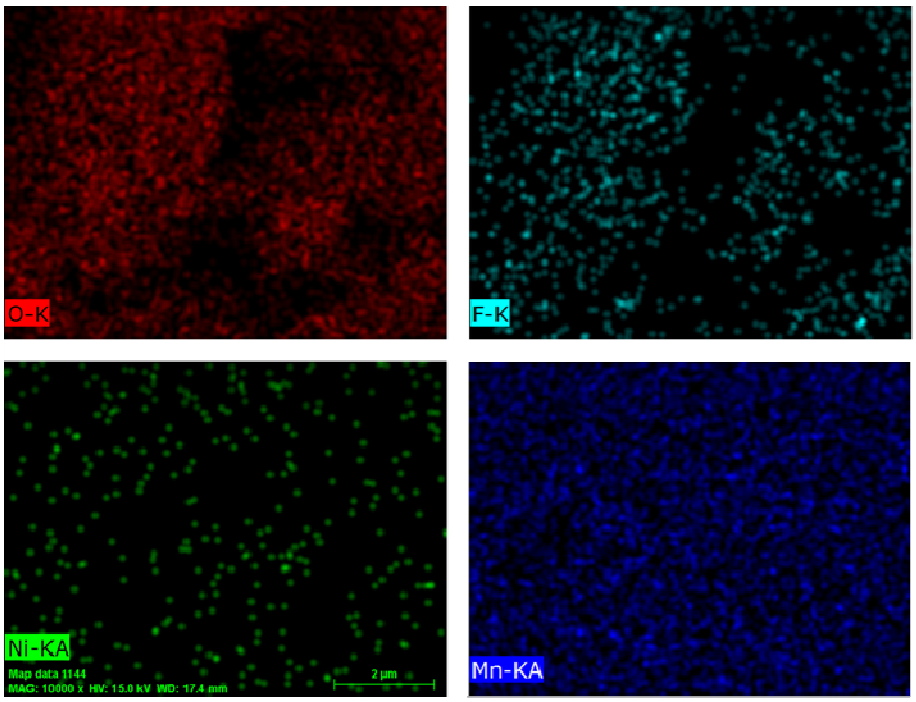

(c)

Fig.4 EDS mapping result of the $LiNi_{0.03}Mn_{1.97}O_{3.95}F_{0.05}$ sample

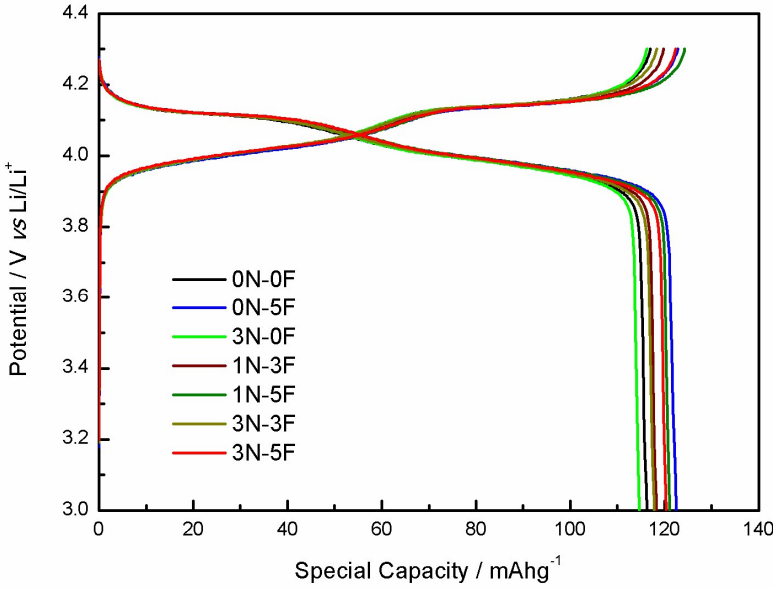

Fig.5 Initial charge-discharge curves of various Ni^{2+} and F^-dual-doped $LiMn_2O_4$samples.

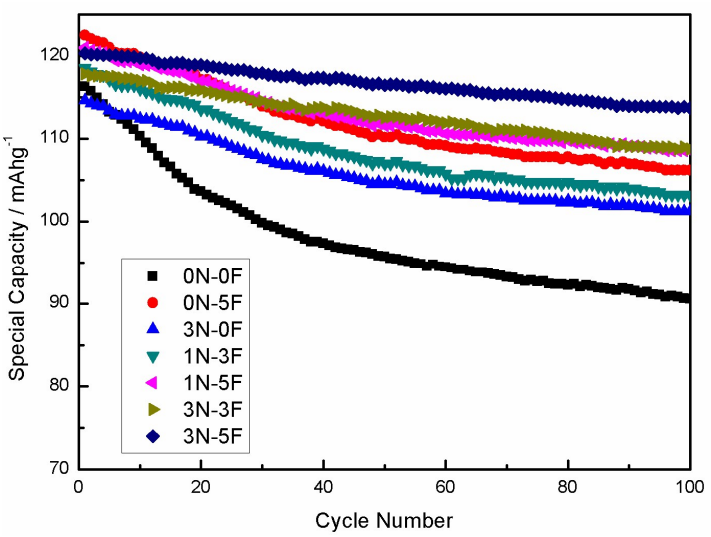

Fig.6 Cyclic performances of Ni^{2+} and F^-dual-doped $LiMn_2O_4$ samples at rate of 1C at room temperature (25 °C).

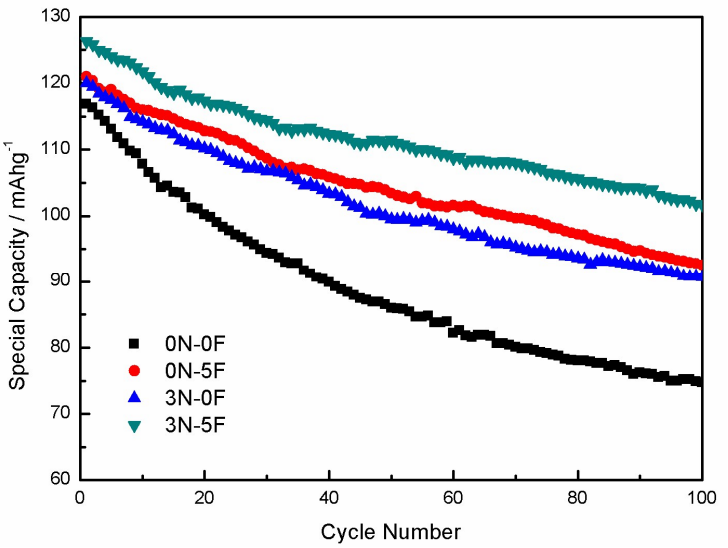

Fig.7 Cyclic performances of Ni^{2+} and F^-dual-doped $LiMn_2O_4$ samplesat rate of 1C at elevated temperature (55 °C).

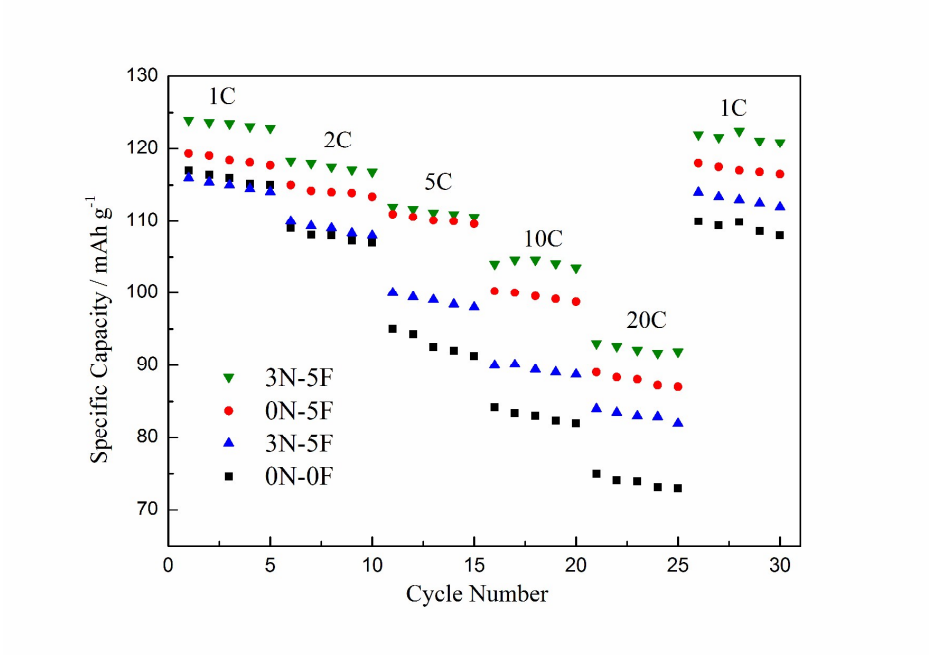

Fig.8 Rate performances of various Ni^{2+} and F^- dual-doped $LiMn_2O_4$ samples at room temperature (25 °C).

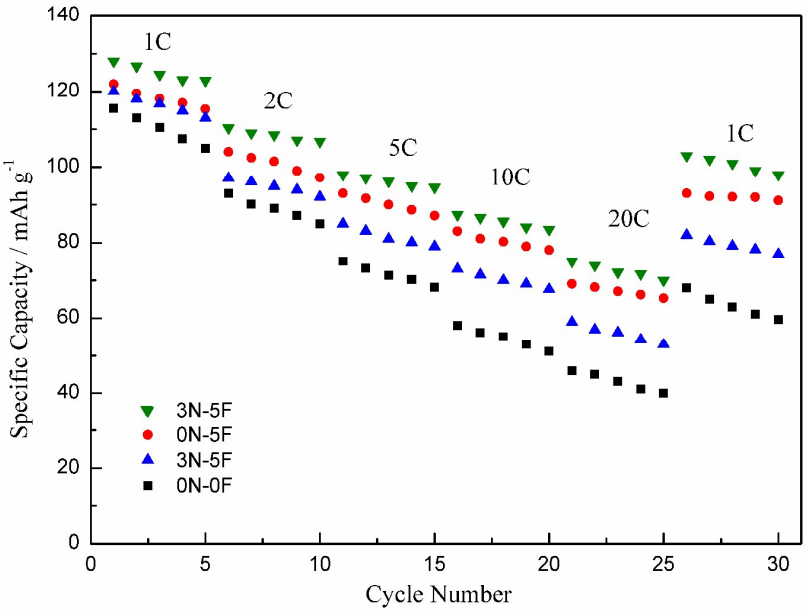

Fig.9 Rate performance of various Ni^{2+} and F^- dual-doped $LiMn_2O_4$ samples at elevated temperature (55 °C).

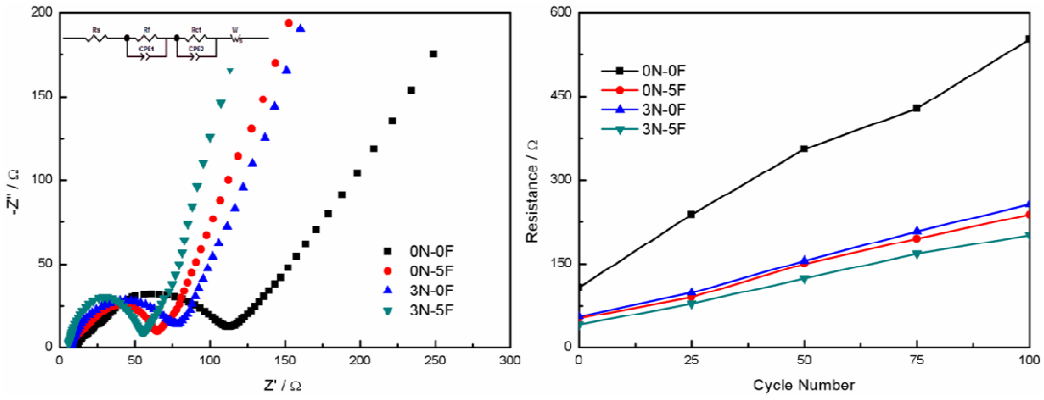

(a) (b)

Fig.10 (a) The Nyquist plots of various Ni^{2+} and F^-dual-doped $LiMn_2O_4$ samples during the first discharge; (b) impedance changes with cycle

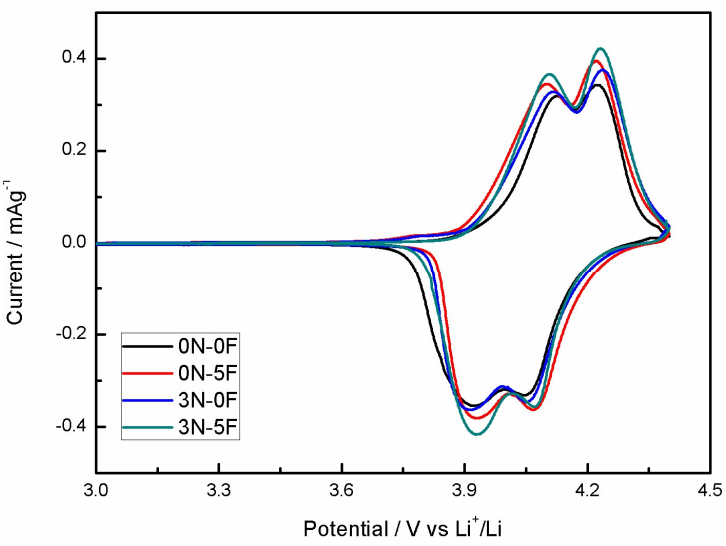

Fig.11 CV curves of various Ni^{2+} and F^- dual-doped $LiMn_2O_4$ samples during the first discharge.

Synthesis and electrochemical performance of Ni and F doped $LiMn_2O_4$ cathode materials

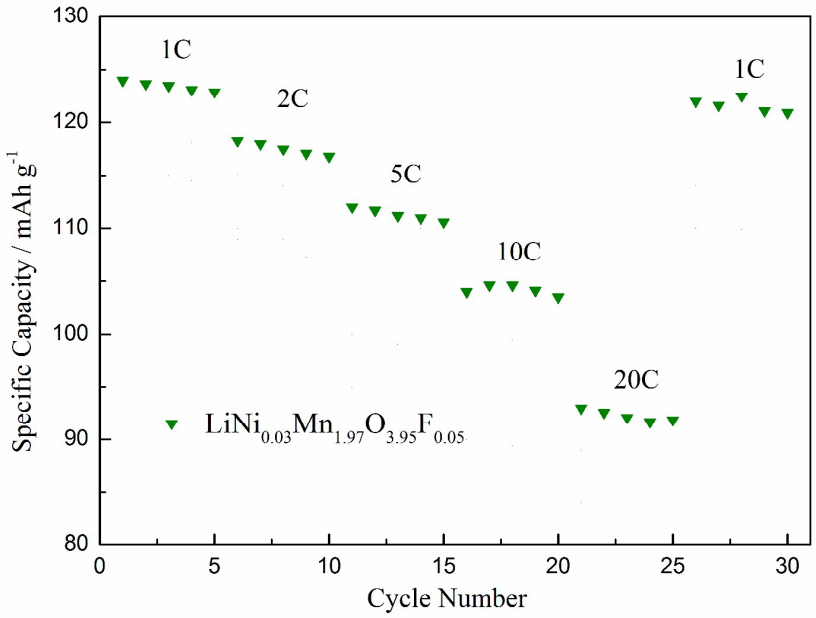

The series of Ni and F ion doped $LiMn_2O_4$ composite cathode materials are synthesized via a sol-gel method. $LiNi_{0.03}Mn_{1.97}O_{3.95}F_{0.05}$ exhibits an excellent electrochemical performance.